ACS APPLIED MATERIALS & INTERFACES

Research Article

www.acsami.org

Photostability of CdSe Quantum Dots Functionalized with Aromatic Dithiocarbamate Ligands

Yizheng Tan,[†] Song Jin, and Robert J. Hamers*

Department of Chemistry, University of Wisconsin—Madison, Madison, Wisconsin 53706, United States

Supporting Information

ABSTRACT: Organic ligands are widely used to enhance the ability of CdSe quantum dots (QDs) to resist photodegradation processes such as photo-oxidation. Because long alkyl chains may adversely affect the performance of QD devices that require fast and efficient charge transfer, shorter aromatic ligands are of increasing interest. In this work, we characterize the formation of phenyl dithiocarbamate (DTC) adducts on CdSe surfaces and the relative effectiveness of different *para*-substituted phenyl dithiocarbamates to enhance the aqueous photostability of CdSe QDs on TiO_2. Optical absorption and photoluminescence measurements show that phenyl DTC ligands can be highly effective at reducing QD photocorrosion in water, and that ligands bearing electron-donating substituents are the most effective. A comparison of the QD photostability resulting from use of ligands bearing DTC versus thiol surface-binding groups shows that the DTC group provides greater QD photostability. Density functional calculations with natural bond order analysis show that the effectiveness of substituted phenyl DTC results from the ability of these ligands to remove positive charge away from the CdSe and to delocalize positive charge on the ligand.

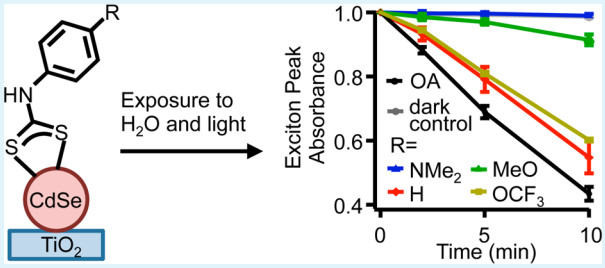

KEYWORDS: *quantum dot, CdSe, hole-transfer, photostability, photoluminescence, dithiocarbamate, surface functionalization*

INTRODUCTION

Chalcogenide quantum dots (QDs) have the potential to be the photoactive material in sensitized solar cells[1] and other optical devices,[2−4] but are prone to photodegradation from water and air.[5−8] Various methods have been utilized to chemically passivate the surface, including surrounding the CdSe with a shell of a large-bandgap material,[9,10] using long hydrophobic hydrocarbon chains,[11] and encapsulating CdSe QDs with organic polymers.[12,13] For QD application that requires fast electrical transport such as in photodetectors, photovoltaic devices, and QD-LEDs, the passivation must be achieved using species that can support electrical conduction, such as short molecular layers.[14,15] Conductive organic ligands significantly affect the QD surface electronic structure[16−18] and could play a significant role in controlling the QD photostability.[19]

Of the ligands that are used in synthesis and manipulation of QDs, thiols are among the most widely used because they bind more strongly than other common ligands such as carboxylic acids, phosphonic acids, and amines.[20] However, passivation with thiols still has inherent problems with photooxidation[21] and labile surface chemistry.[22] Bidentate ligands that have two chelating sulfur groups such as the dithiocarbamate (DTC) group[23] ($R\text{-}NHCS_2^-$) are promising candidates to ensure more stable binding to QDs.[24,25] However, although bidentate ligands are expected to bind more strongly to the QD, there is some evidence that strong ligand binding alone may not necessarily lead to more stable QDs.[21,26] Despite much effort, many questions remain about the relative importance of the ligand binding strength and the influence of the electronic structure of the ligand on QD photostability.

Previous studies of DTCs on CdSe QD surfaces have involved the separate synthesis of the ligand molecule[27] or have functionalized QDs in solution.[24,28] While effective, these approaches require subsequent solvent transfer and other processing steps to make QD adducts with extended surfaces and nanoparticle films. Recent studies have shown that DTC ligands can be assembled in situ on gold substrates under mildly basic conditions.[29,30] This in situ functionalization on a substrate film provides a facile route toward comparison of the different DTC-based ligands on the stability of assemblies of QDs on TiO_2 substrates. Here we report the in situ functionalization of CdSe-TiO_2 films with molecules terminated with DTC groups and utilized this chemistry to explore the influence of molecular structure on QD photostability. Using a series of *para*-substituted, conjugated DTC ligands, we show the increase in QD photostability correlates with the increase in electron-donating ability of the substituent. Finally, we compared the effect of the bidentate DTC versus a monodentate thiol on QD photostability. Our results highlight the importance of charge delocalization on the ligand as a key factor that can substantially stabilize ligand-modified QDs against photodegradation.

Received: September 2, 2013
Accepted: November 20, 2013
Published: November 20, 2013

EXPERIMENTAL SECTION

Chemicals. Trioctylphosphine oxide (TOPO, 99+%), CdO (99.99+% metal basis), oleic acid (OA, 90%), trioctylphosphine (TOP, 90%), selenium, (99.99% metal basis), 4-(trifluoromethoxy)-aniline (98%), aniline (≥99%), *p*-anisidine (≥99%), *N*,*N*-dimethyl-*p*-phenylenediamine (97%), carbon disulfide (anhydrous, ≥99%), triethylamine (TEA, ≥99.5%), and 4-methoxythiophenol (97%) were purchased from Sigma-Aldrich and used without further purification.

Preparation of TiO_2 Nanocrystalline Films. Flourine-doped tin oxide (FTO) coated glass (Hartford glass) was cleaned sequentially with detergent (Alconox), acetone, and ethanol. Porous anatase nanocrystalline TiO_2 films were then screen-printed onto the FTO glass from a commercially available paste (Solaronix T/SP). Each pass of the screen-printing process increases the film thickness by approximately 1 μm. After screen printing, the TiO_2 films were annealed in air using a procedure adapted from literature:[31] at 325 °C for 5 min, at 375 °C for 5 min, at 450 °C for 15 min, and finally at 500 °C for 30 min. Before use, the films were cleaned by heating them at 500 °C for 15 min in air to remove any additional organic contaminants. For XPS and FTIR studies, films from a single screen-print pass were used. Thicker films resulted in interference effects in the FTIR spectra. For photostability studies using UV-Visible spectroscopy, we used samples from two screen-print passes because the increased CdSe QD loading led to higher optical densities. The screen-printing process produced multiple samples with a very constant thickness and mesoporous structure. To ensure maximum reproducibility, each set of data reported here used samples made from a single batch of the screen-printing process.

Synthesis of CdSe QDs. The QDs were synthesized using a procedure adapted from Peng and Peng.[32] While all of the CdSe QDs in this work were made with the procedure described below, due to the slight batch-to-batch variation that naturally comes with QD syntheses, each experimental set was performed with QDs from a single batch. First, 3.1 g of TOPO, 0.24 g of CdO, and 1.9 g of OA were combined in a three-necked flask and heated in an Ar atmosphere until the mixture turned optically clear (~290 °C). Then, the mixture was allowed to cool to ~250 °C, and a solution of TOPSe (made from 1.2 mL TOP and 0.045 g Se) was quickly injected. The temperature dropped to 220 − 230 °C after injection, and the formed QDs were allowed to cool to ~80 °C. The QDs were quenched with toluene and purified four times by precipitation and centrifugation with methanol. The size and concentration of the QDs were determined by UV−visible spectroscopy from the wavelength and absorbance of the first exciton peak, using empirical relationships established by Yu et al.[33] Typically, the QDs from this synthesis procedure were 3−3.2 nm in diameter.

CdSe-TiO_2 Preparation and Ligand Modification. The CdSe QDs were adsorbed directly to the TiO_2 surface without using a linker molecule, following a procedure adapted from literature.[34] Although using a linker may give more control over the QD coverage, studies have shown reduced electron-transfer rate from the linked heterostructures.[34−36] Furthermore, commonly used linkers such as mercapto-alkanoic acids contain sulfur; absence of these sulfur-containing linkers on our CdSe-TiO_2 samples made FTIR and XPS characterization of the DTC functionalization more convenient. To prepare the CdSe-TiO_2 surfaces, the TiO_2 films were immersed in a solution of dichloromethane (DCM) containing a large excess of CdSe QDs[34] (typical concentrations were between 15 and 25 μM) for 24 h, then rinsed with DCM and dried with N_2. In this work, we define the QD molarity as the number of moles of CdSe QDs per liter. To further functionalize these films with DTC molecules, the films were immersed in a stirred, Ar-degassed solution of 50 mM R-aniline (where R designates the different substituent groups as described below), 50 mM CS_2, and 50 mM TEA in methanol for 4 h in the dark. They are then rinsed thoroughly with methanol and dried. To functionalize the CdSe-TiO_2 with 4-methoxythiophenol (MeO-Ph-SH), the films were similarly immersed in an Ar-degassed 50 mM solution of MeO-Ph-SH in methanol for 4 h, then rinsed with methanol and dried.

Fourier-Transform Infrared (FTIR) Spectroscopy. FTIR characterization of the functionalized CdSe-TiO_2 films was performed in single bounce reflection mode with a Vertex 70 (Bruker) FTIR spectrometer using p-polarized light at an incident angle of 50° (for CdSe-TiO_2 samples) or 60° (for CdSe-Si samples) from sample normal and a liquid-nitrogen cooled HgCdTe detector. An identically prepared bare TiO_2 film or bare Si sample served as the reference spectrum for each experiment, and each functionalized sample was measured immediately after the reference sample. This method minimized the effect of atmospheric water and CO_2 on the spectra. Reference spectra of the molecules were measured in transmission mode on ZnSe plates. All measurements were performed using a spectrometer resolution of 4 cm^{-1}. To elucidate infrared absorption features of functionalized QDs at low frequencies, some experiments were performed using Si as a substrate instead of TiO_2. The suspension of as-synthesized CdSe QDs in toluene at a concentration of 83 μM was spin-coated on pieces of Si wafer (Sb-doped, 0.008−0.02 Ω·cm, Addison Engineering) at 1000 rpm for 3 min. For DTC functionalization, the CdSe-Si sample was exposed to 50 mM OCF_3-aniline and 50 mM CS_2 in Ar-degassed methanol for 1 h in the dark. The sample was then rinsed thoroughly with methanol and dried with N_2

X-ray Photoelectron Spectroscopy (XPS). We performed XPS measurements with a custom-built XPS system (Physical Electronics) with an Al Kα source (model 10-610, 1486.6 eV photon energy), toroidal monochromator (model 10-420), and hemispherical analyzer with a 16-channel detector array (model 10-360). Measurements were done at an electron takeoff angle of 45° with an analyzer resolution of 0.1 eV. The resulting XPS peaks were fit to a Voigt function to obtain peak areas.

Water Photostability Studies. Samples were sandwiched into a custom-made cell with a Teflon spacer (127 μm thick) and another piece of FTO. The open region as defined by the spacer was filled with 18 MΩ H_2O (Barnstead Nanopure). The cell has holes to allow for light penetration and absorption measurement without disassembly. Samples were illuminated through the FTO piece and water with light from a solar simulator (Newport 91160, equipped with AM1.5G filters and set to an optical flux of 100 mW/cm^2 as measured by a Scientech calorimeter) after passing through a filter that only allows transmission of wavelengths longer than 475 nm (Newport FSQ-GG475). The flux after the filter was measured to be 81 mW/cm^2. We used the filter to ensure that the light could only be absorbed by the CdSe QDs, and not the TiO_2. Transmission measurements using a UV−visible spectrometer (Shimadzu UV-2401PC) were taken after various durations of illumination.

Photoluminescence (PL). We prepared solution-based QDs functionalized with DTC ligands for the PL experiments. The CdSe QDs were precipitated, centrifuged, and resuspended in chloroform. R-Aniline and CS_2 were added into the solution at a concentration of 50 mM each, and the entire mixture was stirred in the dark for 4 h. To eliminate excess starting reagents, the QDs were precipitated by addition of methanol and then resuspended in chloroform. PL experiments were done using a QD concentration of 1.5 μM with a spectrofluorimeter (ISS K2) using 450 nm as the excitation wavelength.

Calculations. To evaluate the extent of charge transfer between nanoparticle and the ligand, we performed density functional calculations of ligands bonded to a $Cd_{10}Se_{10}$ cluster, using Gaussian 09[37] with the LANL2DZ basis set and effective core potential. A limited set of calculations was performed using a 6-31+G* basis set on the ligand, which yielded very similar results. The extent of charge transfer was evaluated by performing a full optimization of the ligand bonded to the cluster, and then a calculation of the +1 cation at the neutral-optimized geometry. Natural bond orbital analysis[38] was performed to evaluate the charge on individual atoms of the neutral and cation, and the difference between these was used to evaluate the spatial distribution of positive charge resulting from injection of an

electron from the ligand-functionalized CdSe QD into the adjacent TiO_2.

RESULTS

Infrared Characterization of Dithiocarbamate Formation. As a start, we functionalized the CdSe-TiO_2 surfaces using an aniline derivative having an $-OCF_3$ substituent, OCF_3-aniline; under the conditions of our experiment, this molecule reacts to form the dithiocarbamate, OCF_3-Ph-DTC, which then adsorbs to the CdSe surface. The OCF_3-Ph-DTC structure is illustrated in Figure 1e. The CF_3 group serves as a molecular tag, since it has relatively unique absorption features in the IR at ~1200−1300 cm^{-1} and the F atoms facilitate analysis via XPS with no interferences. Because prior studies have generally found that dithiocarbamate formation is enhanced in the presence of a base such as TEA,[29,39] we also evaluated the effect of this base on the formation of DTC monolayers on CdSe QDs. Figure 1 shows IR and XPS spectra of a CdSe-TiO_2 sample after exposure to the full reactant mixture of OCF_3-aniline, TEA, and CS_2 ("OCF_3-anil+TEA+CS_2") for 4 h, along with similar samples that were exposed to reactant mixtures in which either the TEA ("No TEA") or the CS_2 ("No CS_2") was eliminated. Also shown are a control sample ("unreacted") consisting of OA-capped CdSe QDs on TiO_2 with no further modification, and a spectrum of the neat parent OCF_3-aniline compound. In these spectra, the reference sample for calculating the absorbances was a bare TiO_2 nanoparticle film. In Figure 1a, the sample that was exposed to the full OCF_3-anil+TEA+CS_2 mixture and an identical sample that was exposed to this mixture but without TEA ("No TEA") both show peaks at 1510, 1271, and 1227 cm^{-1}. The peak at 1510 cm^{-1} is in the typical range of an aromatic ring stretch. The modes at 1271 and 1227 cm^{-1} are in good agreement with the C−F modes previously reported for trifluoromethoxybenzene, which yielded a strong feature at 1274 cm^{-1} and a weaker mode at 1274 cm^{-1}.[40] Surprisingly, the FTIR spectra indicate that the sample made in the absence of TEA gives rise to stronger features than the one including the base. The "No CS_2" sample shows no sharp infrared features from the CF_3 or C═C stretches from OCF_3-aniline, while the "unreacted" control sample (OA-capped CdSe QD on TiO_2) yields only broad peaks at 1535 and 1412 cm^{-1} that arise from the carboxylate stretching modes of the OA molecules that cap the as-synthesized QDs.[41] Figure 1a also shows the transmission IR spectrum of neat OCF_3-aniline. The IR spectrum of this pure liquid shows several prominent peaks at 1350−1150 cm^{-1} that arise from the CF_3 group, and a peak at 1510 cm^{-1} that arises from one of the aromatic C═C stretches.

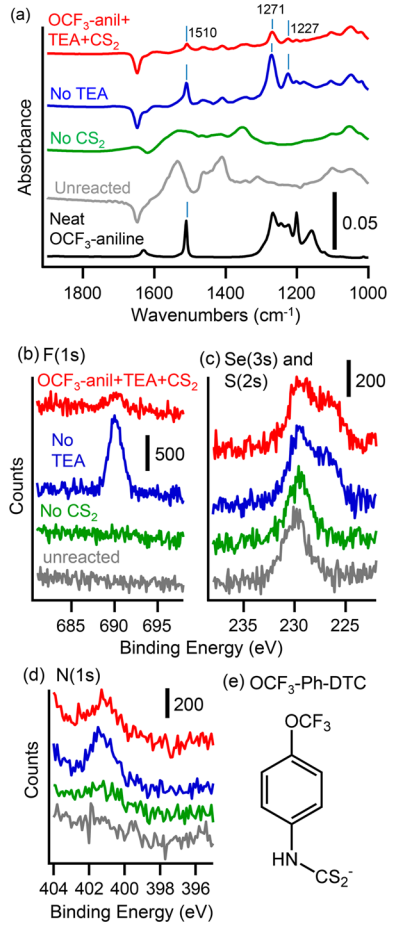

Figure 1. (a) FTIR spectra of OCF_3-Ph-DTC functionalization. The neat OCF_3-aniline spectrum is included as reference. The sample with full functionalization conditions labeled as "OCF_3-anil+TEA+CS_2". The "No CS_2" spectrum is the control with the CS_2 left out, while the "No TEA" spectrum is control with TEA left out. (b−d) XPS spectra of the (b) F(1s), (c) Se(3s) and S(2s), as well as (d) N(1s) regions of the functionalization, along with the proper controls. (e) Structure of the DTC molecule formed from the reaction between OCF_3-aniline and CS_2.

XPS Characterization of Dithiocarbamate Formation. XPS measurements further confirmed binding of the molecules via the DTC linkage. Figure 1b−d shows the F(1s), Se(3s)/S(2s), and N(1s) spectra, respectively, from samples exposed to OCF_3-aniline, TEA, and CS_2, along with control samples like those above. The XPS data show that significant F(1s) intensity is present only when both OCF_3-aniline and CS_2 are present. XPS analysis of the DTC functionalization is complicated by the fact that the S(2s) and Se(3s) core-level peaks are overlapped, making quantitative analysis using these peaks difficult. The unmodified CdSe-TiO_2 control sample, which contained no sulfur, exhibited a single peak at 229.5 eV which

we therefore assigned to the Se(3s) peak of bulk CdSe. Samples that were exposed to OCF_3-aniline and CS_2 exhibited a second feature at 226.8 eV that we therefore assigned to the S(2s) peak of the DTC linkage. This peak occurred only on samples that were exposed to CS_2; that is, the "OCF_3-anil+CS_2+TEA" and the "No TEA" samples each had this sulfur peak, but the "No CS_2" control did not. The N(1s) region was riding on the tail edge of the large Cd($3d_{5/2}$) peak, resulting in a rising background. However, there was a clear nitrogen peak in each of the "OCF_3-anil+CS_2+TEA" and the "No TEA" samples.

The XPS peak areas of the F(1s), S(2s), and N(1s) can be used to estimate the stoichiometry of the adsorbed molecules after correcting the raw areas by the atomic sensitivity factor of each element. For the "No TEA" sample, peak area ratios were A_{F1s}/A_{N1s} = 3.2 and A_{F1s}/A_{S2s} = 1.3; these values are close to the values of A_{F1s}/A_{N1s} = 3 and A_{F1s}/A_{S2s}= 1.5 expected from the stoichiometry of the OCF_3-Ph-DTC molecule. When TEA base was included ("OCF_3-anil+CS_2+TEA"), the low intensity of the N(1s) and S(2s) signals precluded accurate measurement of these ratios. The relative amounts of each molecule on the surface were estimated from the F(1s) and Cd intensities. The A_{F1s}/A_{Cd} area ratio was 0.4 for the sample without TEA exposure but was only 0.07 when TEA was included as a reagent, demonstrating (in agreement with the FTIR data) that the presence of TEA base inhibits formation of the dithiocarbamate surface complex. For the "OCF_3-anil +CS_2+TEA" sample, the area ratio is A_{F1s}/A_{N1s} = 1.2. This low A_{F1s}/A_{N1s} ratio shows that while TEA inhibits dithiocarbamate formation, there is excess nitrogen on the surface and could indicate that some TEA base is also binding, blocking functionalization of the DTC. Additionally, experiments in which we varied the TEA concentration in the reaction showed a general decrease in the extent of functionalization as the concentration of TEA increased (see SI). This functionalization condition differs from the typical organic synthesis of DTC molecules, in which basic conditions is required.[39,42]

Because of the small diameter of the spherical nanoparticle and because the electron escape depths are comparable to the nanoparticle diameters, quantitative analysis of absolute molecular coverage from XPS data requires explicitly accounting for the shape and size of the nanoparticles and the electron scattering within the nanoparticle and the adsorbed molecular layer. We previously used numerical integration to calculate the expected intensity ratios for a spherical nanoparticle surrounded by a molecular layer including scattering effects.[19] Here, we have adapted this approach to include the sulfur head group as an interface between the organic ligand and CdSe core. Using this approach, we determined that the molecular coverage was 1.7×10^{14} molecule/cm^2 based on the S/Cd peak area ratio of the "No TEA" sample. This sample, with the TEA base left out in the functionalization procedure, was the one that yielded the correct stoichiometric ratios of the OCF_3-Ph-DTC molecule as described above.

Binding Mode of DTC on CdSe. Since the DTC ligands have two sulfurs to bind to the surface of the CdSe, the DTC group can bind in a bidentate or a monodentate fashion. There have been many studies of metal ion-ligand complexes including X-ray crystallography data that showed the bidentate configuration for Cd^{2+} ion chelated to DTCs,[39,43,44] but there has been no clear evidence that this configuration would be the most stable for DTCs binding to bulk CdSe surfaces or QDs. In the prior studies, the splitting between the asymmetric and symmetric C═S vibrational modes at 950−1050 cm^{-1} has been used to differentiate between the two binding configurations of the metal-ligand complexes. The appearance of a single mode or modes split by <20 cm^{-1} was used to indicate bidentate binding of the DTC group.[43,45] The few published FTIR spectra of DTCs bound to CdSe QDs are inconclusive; they verified the presence of the C═S stretches, but did not discuss binding modes in detail.[46,47] We attempted to determine the binding mode of our DTC ligand functionalization. In order to eliminate the large interferences in the IR at 830−990 cm^{-1} that arise in Figure 1a from the TiO_2 substrate (see Figure S2 in the SI), for this study we used CdSe QDs that were deposited on a silicon substrate. Figure 2a shows the resulting FTIR spectra

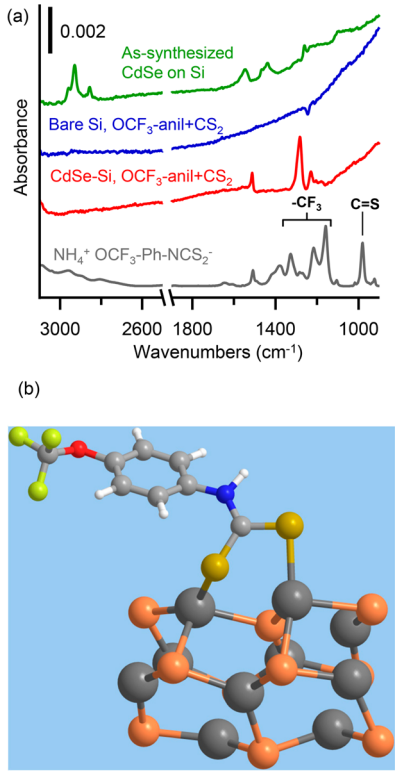

Figure 2. (a) FTIR spectra of OCF_3−Ph-DTC functionalization on CdSe nanoparticles on Si substrates. The unmodified sample shows peaks from the OA ligands of the as-synthesized CdSe. The absence of relevant peaks from the DTC functionalization procedure indicates no binding on the bare Si control. Spectrum of the pure NH_4^+ OCF_3−Ph-DTC^- salt is included as reference. (b) Structure of the OCF_3-Ph-DTC functionalized on a $Cd_{10}Se_{10}$ cluster after geometry optimization, showing the bidentate nature of the binding.

along with the associated controls. As a reference, we synthesized the pure OCF_3-Ph-DTC compound according to literature[27] to determine the position of the C═S stretch and assigned the strong peak at 980 cm^{-1} as the C═S. The sample of "as-synthesized" CdSe deposited on Si shows the aliphatic vibrations (2850−2920 cm^{-1}), vinyl, and carboxylate peaks characteristic of the OA ligand. We confirmed that the DTC molecules do not bind onto bare Si; therefore the DTCs are bound only onto the CdSe QDs. When the QDs were exposed to the OCF_3-aniline and CS_2 to form the surface DTC functionality, we observed the peaks arising from the CF_3 group and the C═C of the aromatic ring. However, no distinct features were observed in the C═S region. Crudely, one would expect that a monodentate bonding configuration would yield a

detectable C═S absorption at a frequency similar to that of the parent molecule. When comparing the relative intensities of the CF_3 and the C═S peaks in the pure DTC compound versus the relative intensities of the same features in our CdSe functionalized sample, the absence of a strong C═S peak suggests bidentate binding in our DTC ligands. The C═S stretches appear to also be relatively weak in the published FTIR data of CdSe-DTCs.[46,47]

Density Functional Calculations of Ligands on CdSe Cluster. On CdSe, the ~2.96 Å bond distance between the two S atoms of a N-CS_2^{-1} free ligand[48] is a poor match to the 4.30 Å distance between adjacent Cd atoms and the 2.64 Å distance between adjacent Cd and Se atoms.[49] To evaluate the most likely bonding geometry of DTC molecules on CdSe, we calculated the relative energies of various DTC adducts with a $Cd_{10}Se_{10}$ cluster using Gaussian 09.[37] In these calculations, we pre-poised 4-trifluoromethoxy-1-dithiocarbamate molecule on the cluster at various positions including the monodentate and bidentate bonding configurations, and then performed total energy minimizations for each completed molecule-cluster adduct. While several local minima were found, the lowest-energy configuration, as depicted in Figure 2b, has the two S atoms bonded to adjacent Cd atoms. The monodentate configuration (with one S atom bonded to a Cd and the other pointing away from the cluster) and a second bidentate geometry involving bonding to adjacent Cd and Se atoms were both significantly higher in energy (~0.3 eV) compared with thermal energies (kT = 0.026 eV at 300 K). Thus, we anticipate that the majority of molecules are likely in the bidentate binding to two Cd atoms or similar configurations.

Photostability of Dithiocarbamate-Functionalized CdSe. Using the functionalization procedure as described above for the OCF_3-Ph-DTC, we performed similar experiments to other *para*-substituted phenyl groups, R-Ph-DTCs, R = H, MeO, and NMe_2. FTIR spectra of these samples are shown in the Supporting Information. All reactions were done at a fixed concentration (50 mM each of R-aniline and CS_2 in methanol) without the addition of TEA base and using the same reaction times. At these concentrations, the best functionalization was achieved using a reaction time of 4 h. At longer reaction times, we found that the DTC molecules etched the CdSe QDs (see SI for grafting kinetics and detailed discussion). We investigated the aqueous photostability of CdSe-TiO_2 samples functionalized with a series of *para*-substituted phenyl DTC ligands. Figure 3a shows visible absorption spectra of the OCF_3-Ph-DTC functionalized sample obtained consecutively at various time points, up to 10 min of exposure to light and water. At 0 min, the data show a peak at 559 nm corresponding to the first exciton peak. After exposure to water and light, the peak shifted and broadened, and its amplitude decreased, indicating photodegradation to the QDs. Exposure to light was needed to induce this degradation; no change in exciton peak energy or width was observed for a control sample that was kept in the dark, consistent with previous results.[19]

To compare how different ligands affected the QD photostability, for each QD-ligand adduct, we extracted the amplitude of the first exciton peak to quantify the rate of degradation. The raw absorption spectrum was fit to a Gaussian with a baseline as shown in Figure 3b. The baseline was fit to a cubic function, following previous reports.[50] For each sample, we used the amplitude derived from the Gaussian fit, A, at each time point and normalized it by its value at time = 0, A_0, to obtain the fraction remaining or A/A_0. Figure 3c shows the plot of A/A_0 values at different exposure times for each set of ligand-functionalized CdSe. The error bars are standard deviations from four equivalently prepared samples. This plot also includes similar results for an unmodified (OA-functionalized) CdSe-TiO_2 sample, and a dark control of an OA-functionalized sample. The OA sample exhibited the most rapid photodegradation in water of all of the ligands studied here. The data in Figure 3c show that the rate of QD photodegradation is strongly dependent on the identity of the *para*-substituent of the R-Ph-DTC functionalized CdSe QD. Of these samples, the stability trend was: R = NMe_2 > MeO > H ≈ OCF_3.

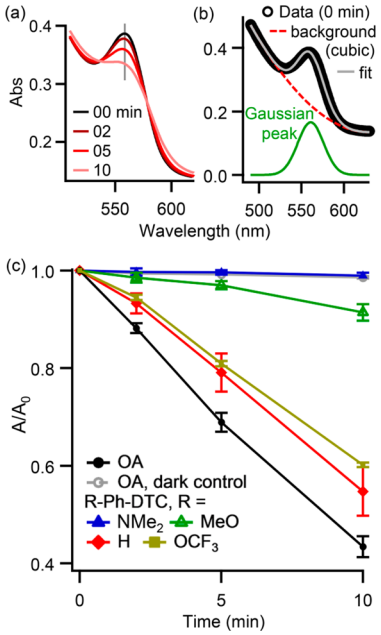

Figure 3. Water photostability of CdSe-TiO_2 samples functionalized with R-Ph-DTCs, R = OCF_3, H, MeO, and NMe_2. (a) Transmission visible absorbance spectra of the R = OCF_3 sample at 0, 2, 5, and 10 min exposure to light and water. (b) Fitting procedure to extract the first exciton peak height, A. The rising baseline was fit to a cubic function, and the peak was fit to a Gaussian (c) A/A_0 values plotted as a function of exposure time for all R substituents. Also included is data from an OA-functionalized sample and from the dark control of an OA-functionalized sample.

Electron Injection and Fluorescence Quenching. One explanation for the enhanced photostability with increasing electron-donating ligands is that electron-rich ligands are more effective at transferring electrons to the CdSe core (or equivalently, to transfer a hole from the CdSe to the ligands). Prior studies have established that the photodegradation of CdSe QDs arises primarily from the fact that when CdSe is excited and electron-hole pairs are created, the holes in the valence band are able to oxidize Se^{2-} ions at the CdSe surface to Se^0 and higher oxy-anions, with concurrent loss of Cd^{2+} ions into solution.[5,51] Consequently, rapid injection of electrons from an external substituent group into the valence band (or equivalently, transfer of the valence band hole from the CdSe to the ligands) can reduce photodegradation. The efficiency of this ligand-to-CdSe electron transfer process can be measured with PL quenching experiments. The transfer of an electron from the ligand to the excited CdSe QD leaves no low-energy unoccupied level for the excited electron to radiatively relax. Quenching via this process has been observed previously with

CdSe QDs functionalized with thiols[52−55] and dithiocarbamates;[24,46] in both cases, as photoexcited holes are trapped in the ligand, the radiative recombination pathways of the QD decreased.[56]

To test whether the ability of electron-donating DTC ligands to enhance photostability was correlated with their hole transfer efficiency, we performed PL of freshly-prepared CdSe QDs functionalized with R-Ph-DTCs, (where R = OCF_3, H, and MeO) suspended in chloroform. For the PL experiments, we did not include the DTC molecule with the R = NMe_2 substituent because the parent NMe_2-Ph molecule is visibly colored. Figure 4a shows the photoluminescence intensity from

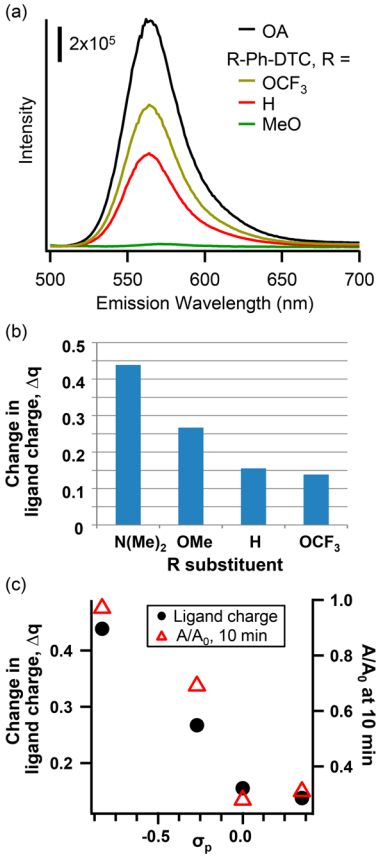

Figure 4. (a) PL spectra of the CdSe suspension in chloroform functionalized with R-Ph-DTCs, R = OCF_3, H, and MeO. (b) The change in charge on DTC ligand charge (units of 1.602×10^{-19} C) between neutral and cationic clusters as calculated from NBO analysis. (c) NBO change in ligand charge ploted as a function of the Hammett parameter σ_p of ligand substituent group. Also included are the A/A_0 values (after 10 min of exposure to light and water) of the DTC-functionalized CdSe-TiO_2.

CdSe QDs functionalized with these DTC ligands, using an excitation wavelength of 450 nm. The PL spectrum of an OA-capped QD sample is also shown for comparison. Overall, the DTC ligands quenched the PL as compared to the as-made (OA-capped) sample. PL quenching efficiency trended as follows: R= OCF_3 (amplitude of the PL peak is 63% of that of the OA) < H (41% of OA) ≪ MeO (1.4% of OA). To eliminate the effects of unreacted anilines that did not form DTC linkages, we also performed control experiments with exposure of QD suspensions to the corresponding anilines only (no CS_2 added); these samples did not induce any significant changes in the photoluminescence signal. The PL trend suggests that increasing the electron-donating ability of the DTC ligand results in increased hole transfer efficiency from the QD into the ligand.

To evaluate the relationship between stability and the electronic structure of the ligands, we used the natural bond order (NBO) analysis.[38] NBO analysis was performed on the optimized structures to determine the partitioning of charge between molecule and $Cd_{10}Se_{10}$ cluster. In applications such as QD-sensitized solar cells, the QD-ligand adduct injects charge in an adjacent electron acceptor (such as TiO_2), leaving it with a positive charge that results in high reactivity toward deleterious oxidation processes. Consequently, we evaluated the NBO "natural charge" on each atom in the energy-minimized molecule/cluster adduct in the neutral state and in the cation state at the neutral-optimized geometry. We then determined the *change* in atomic charge upon going from the neutral to the cation as a measure of the spatial distribution of positive charge after the CdSe-ligand adduct is excited and injects an electron into the adjacent TiO_2. Figure 4b shows results of the four ligands studied here. These NBO results show that the ability to sequester charge from the CdSe onto the ligands trended as R= NMe_2 (best) > MeO > H ~ OCF_3. This trend is identical to that obtained in our experimental photostability measurements and the photoluminescence quenching experiments (Figure 4a), indicating that the photostability of CdSe QDs is closely correlated with the ability to remove the positive hole that is left after electron injection. We also calculated the atomic distribution of charge for the various ligands and found that the amount of charge on the S atoms is nearly identical for each of ligands, while dimethlyamino dithiocarbamate was most effect at delocalizing the charge onto the ligand. (SI, Figure S10).

The computational results in Figure 4b and c correspond to the lowest-energy bonding configuration of MeO-Ph-DTC as described above. To test the sensitivity of the calculations to various starting conditions, we also calculated the charge distributions for several of the higher-energy monodentate and bidentate binding configurations described above. The charge distributions were also calculated for a modified cluster having hydrogen atoms terminating the edges of the cluster except for the two Cd and two Se atoms nearest the bonding site. In each case, the amount of charge localized on the molecule was very similar to the values reported here, yielding a consistent trend. The fact that these control experiments yielded similar results to those depicted in Figure 4b indicates that the charge transfer between the cluster and the molecules is not strongly dependent on the detailed nature of binding between the molecule and the cluster. This conclusion is further supported by the data in Figure 4c, which show how the calculated molecular charge and the experimental exciton peak heights (characterized as the A/A_0 values measured in the photostability studies above) change with the Hammett parameter of the substitutional group. The Hammett parameter, σ_p,[57] is widely used to qualitatively compare how the electron-donating ability of molecular ligands influence chemical reactivity. The σ_p values are referenced to the H-substituent (i.e., σ_p of R = H is 0 by definition), and are more negative for more electron-donating substituents. Previous studies have established values of $\sigma_p = -0.83$ (R = NMe_2), $\sigma_p = -0.27$ (R = MeO), and σ_p = 0.35 (R = OCF_3).[58] Thus, the trend in photostability closely tracks the trend in electron-donating character, with *para*-substituents having the most negative σ_p providing the greatest

ability to resist photodegradation. Clearly, there is a very strong correlation between these.

Comparison of Dithiocarbamate and Thiol Linkages. We originally hypothesized that the dithiocarbamate ligand might provide enhanced stability compared with simple thiols. While the DTC molecule having the -NMe_2 substituent group yielded the best photostability, because the parent amine (i.e., NMe_2-Ph-NH_2) absorbs in the same region as the CdSe QD first exciton peak (see SI) we chose molecules bearing the MeO substituent instead. Neither the MeO-Ph-NH_2 parent molecule nor the MeO-Ph-SH has any significant absorption features in the 475−600 nm region. Water stability measurements like those reported in Figure 3c were performed. Figure 5a shows

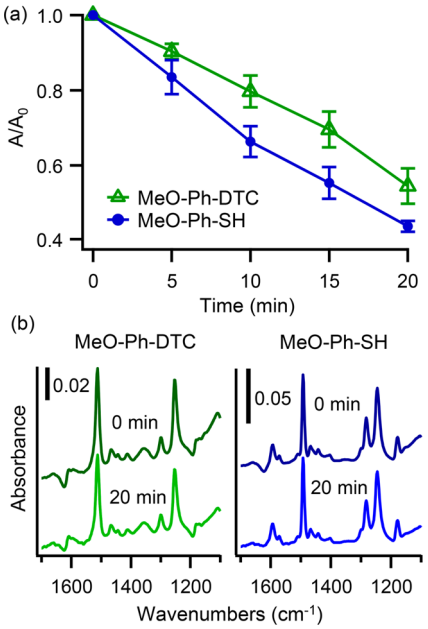

Figure 5. (a) Water photostability of the MeO-Ph-DTC versus MeO-Ph-SH. The graph shows A/A_0 values as a function of exposure time, up to 20 min. (b) Ligand desorption studies in the dark. FTIR spectra of the DTC and the SH binding group at 0 min and after 20 min of exposure to water, showing no significant change in the absence of illumination.

the resulting A/A_0 values versus duration of exposure to water. The data show that the DTC ligand is slightly more stable than the thiol. To see whether the enhanced stability were purely from differences in ligand (DTC versus thiol) desorption kinetics from the QDs, we took FTIR measurements of the samples before and after exposure to water in the dark. Figure 5b shows the FTIR spectra of DTC or thiol bound CdSe at 0 and 20 min of exposure to water, but not exposed to light. The characteristic features of the surface-bound ligands remained the same, indicating no significant desorption of ligands in the time scale of the experiment. To investigate whether this effect simply resulted from molecular packing differences in the thiol and DTC, XPS was used to quantitatively compare the molecular densities. XPS analysis of the S to Cd ratio yielded 1.9 DTC molecules/nm^2 and 2.3 thiol molecules/nm^2. These data show that the DTC has a slightly lower packing density than the equivalent thiol, but DTC still yields slightly greater stability.

DISCUSSION

Our experimental results show several important pieces of information. First, the data demonstrate successful in situ formation of dithiocarbamate ligands on CdSe-TiO_2 heterostructures, and that contrary to prior studies on gold[29] the best layers are obtained without addition of a base. Second, the *para*-substituents on the DTC molecule have a large influence on the water photostability of CdSe QDs, with electron-donating substituents providing higher stability. Finally, a comparison of thiol and DTC binding groups yielded higher stability with the DTC group.

We first address the role of the TEA base on DTC functionalization to CdSe surfaces. The synthesis of DTC molecules is typically done in the presence of base as the proton acceptor because the DTC formation reaction R-NH_2 + CS_2 → R-$NHCS_2^-$ + H^+ (where "R" represents an aliphatic or aromatic group) produces H^+ as a product, and the presence of a base to sequester the H^+ shifts the equilibrium toward the right.[23,42] However, our results show that formation of DTC complexes on CdSe QDs is facile without added base, and that the addition of TEA even *inhibits* the surface functionalization. We attribute the deleterious effect of TEA to the fact that amines are known to bind onto CdSe QDs.[59−62] Consequently, when TEA is used, the TEA competes with the DTC ligands for the available surface sites. Although TEA may assist in the formation of the dithiocarbamate complex in solution, our results show that it inhibits binding of the complexes to the CdSe surface.

The stability of the ligand-modified nanoparticles is controlled by both thermodynamics and by kinetic processes such as desorption and the penetration of water to the ligand−nanoparticle interface.[21,63] In the absence of photochemical processes, molecules bearing multiple independent binding groups are generally expected to exhibit greater stability relative to molecules bearing only a single binding group because entropy disfavors the simultaneous breaking of multiple molecule−surface bonds.[63,64] However, because stability in water is likely controlled by penetration of water to the ligand−nanoparticle interface,[21] the remainder of the ligand also plays a critical role. Stability in aqueous media is best under conditions where the ligands can pack tightly on the surface, thereby limiting diffusion of water to the nanoparticle-ligand.[21] These factors suggest that highest stability can likely be achieved using ligands with small, tightly binding surface-binding groups that can provide a combination of high binding strength and high molecular packing density. Temperature-programmed desorption studies in ultrahigh vacuum found that dithiocarbamates required a higher temperature to desorb compared with simpler thiols,[65] indicating that dithiocarbamates are bound more strongly than thiols.

The *photo*stability of ligand-modified QDs is complex because there are multiple mechanisms for degradation. Previous studies have shown that under conditions where a CdSe QD injects an electron into an adjacent medium (such as TiO_2), the stability of the ligand-QD adduct is controlled by the fact that the hole remaining on the QD can oxidize surface selenium atoms or surface-binding groups of the ligand (such as thiols).[21,51] Both processes can lead to removal of the surface ligands, leaving the QD more susceptible to attack. In our previous study, we showed that adsorption of aromatic thiols bearing electron-donating substituent groups greatly enhanced the photostability of CdSe QD-TiO_2 adducts compared with

simple alkanethiol ligands.[19] We further showed that in such adducts the positive charge of the CdSe-ligand adduct (to simulate stability under conditions where excited electrons are injected into TiO_2) is extensively delocalized onto the aromatic ring of the ligand molecule, thereby preventing oxidation of the thiol linkage.[19] Our current work extends these findings to include DTC linkages, as we observe that the DTC linkage, especially when coupled to an aromatic ring and electron-donating ligands, can be highly effective at stabilizing the CdSe QDs.

The ability to delocalize the charge is controlled in part by the surface binding group. Prior studies of conductivity through conjugated molecules on Au[65,66] and CdSe[46] surfaces reported that DTC linkages provided higher conductivity than thiol groups. The higher conductivity when using the DTC linker was attributed to increased delocalization of the molecular orbital between the junction and the Au or CdSe material.

Our data suggest that the electronic structure of the molecule plays a dominant role in controlling photostability of DTC-CdSe-TiO_2 adducts. Consistent with our previous work, our present study shows that the CdSe-DTC photostability is strongly dependent on the ability of the ligand molecules to delocalize the positive charge that is left after excitation and electron injection from the CdSe into the TiO_2. The *para*-substituent of phenyl DTCs with a more negative σ_p (more electron-donating) substituent led to the greater stability. Our measurements and calculations have some significant differences with recent work by Frederick et al.[27] They performed density functional calculations of the electronic structure of different *para*-substituted phenyl dithiocarbamates linked to Cd_5Se_4 clusters and concluded that the exciton state that is formed upon excitation is more effectively delocalized onto the ligands when the ligands had electron-*withdrawing* substituents. This apparent inconsistency with our results can be resolved by noting that the exciton state has a very short lifetime, and that under conditions relevant for most applications (such as QD-sensitized solar cells) the exciton injects electrons into an adjacent electron-accepting material (such as TiO_2), leaving the QD and the ligand with a net positive charge. This net positive charge is ultimately responsible for the photodegradation of the QDs. Thus, instead of calculating the distribution of charges in the neutral (exciton) state, our calculations focused on the spatial distribution of charge after electron emission, when the DTC-CdSe adduct has a net positive charge. Our density functional calculations of the charge distribution in this *cationic* state clearly show that the net positive charge is more extensively delocalized onto the ligand when bearing electron-donating ligands, in agreement with our experimental results of increased photostabilty. Thus, the spatial distribution of the initially excited exciton state is less important than the distribution of positive charge remaining after electron injection. Ultimately, our experimental and computational work suggests that the electronic structure of the linker and the ligand itself are both very important.

CONCLUSIONS

Our studies show that aromatic dithiocarbamates can be very effective at enhancing photochemical stability of CdSe QDs in water, with greatest stability achieved when the aromatic ring is functionalized with electron-donating substituents. The surface binding group also plays a small role, as DTC-functionalized QDs showed slightly improved stability compared with the aromatic thiols investigated earlier,[19] while XPS measurements show similar packing densities for molecules bearing DTC and thiol linkages. Our current study, like our previous investigation using thiols, shows that the ability of the ligand to delocalize the positive charge onto the ligand, away from the QD core and the surface linking group, plays a central role in the ability of ligands to stabilize CdSe against photodegradation.

ASSOCIATED CONTENT

Supporting Information

Additional control experiments for the functionalization of OCF_3-Ph-DTCs on CdSe-TiO_2 samples, functionalization of R-Ph-DTCs (where R = H, MeO, and NMe_2 on CdSe-TiO_2 surfaces, grafting kinetics of OCF_3−Ph-DTC on CdSe, grafting extent as a function of TEA concentration, representative XPS spectrum of the Cd(3d) region, schematic of the photodegradation cell, absorption spectra of the R-Ph-DTC functionalized CdSe-TiO_2 samples, longer term photostability studies of the NMe_2-Ph-DTC functionalized CdSe-TiO_2, and atomic coordinates for neutral-optimized ligand-CdSe clusters. This material is available free of charge via the Internet at http://pubs.acs.org/.

AUTHOR INFORMATION

Corresponding Author

*E-mail: rjhamers@wisc.edu.

Present Address

[†]Y.T.: The Molecular Foundry, Lawrence Berkeley National Laboratory, Berkeley, California 94720.

Notes

The authors declare no competing financial interest.

ACKNOWLEDGMENTS

We are grateful to Caroline English, Kyle Czech, and Prof. John Wright for helpful discussions and insights. This work was supported by the Department of Energy, Office of Basic Energy Sciences, Division of Materials Sciences and Engineering, under Award DE-FG02-09ER46664.

REFERENCES

(1) Kamat, P. V. *J. Phys. Chem. Lett.* **2013**, *4*, 908−918.
(2) Colvin, V. L.; Schlamp, M. C.; Alivisatos, A. P. *Nature* **1994**, *370*, 354−357.
(3) Konstantatos, G.; Howard, I.; Fischer, A.; Hoogland, S.; Clifford, J.; Klem, E.; Levina, L.; Sargent, E. H. *Nature* **2006**, *442*, 180−183.
(4) Shirasaki, Y.; Supran, G. J.; Bawendi, M. G.; Bulovic, V. *Nat. Photonics* **2013**, *7*, 13−23.
(5) Katari, J. E. B.; Colvin, V. L.; Alivisatos, A. P. *J. Phys. Chem.* **1994**, *98*, 4109−4117.
(6) Sykora, M.; Koposov, A. Y.; McGuire, J. A.; Schulze, R. K.; Tretiak, O.; Pietryga, J. M.; Klimov, V. I. *ACS Nano* **2010**, *4*, 2021−2034.
(7) Tvrdy, K.; Kamat, P. V. *J. Phys. Chem. A* **2009**, *113*, 3765−3772.
(8) Židek, K.; Zheng, K.; Chábera, P.; Abdellah, M.; Pullerits, T. *Appl. Phys. Lett.* **2012**, *100*, 243111.
(9) Barea, E. M.; Shalom, M.; Gimenez, S.; Hod, I.; Mora-Sero, I.; Zaban, A.; Bisquert, J. *J. Am. Chem. Soc.* **2010**, *132*, 6834−6839.
(10) Ihly, R.; Tolentino, J.; Liu, Y.; Gibbs, M.; Law, M. *ACS Nano* **2011**, *5*, 8175−8186.
(11) Wang, Y. A.; Li, J. J.; Chen, H. Y.; Peng, X. G. *J. Am. Chem. Soc.* **2002**, *124*, 2293−2298.
(12) Potapova, I.; Mruk, R.; Prehl, S.; Zentel, R.; Basche, T.; Mews, A. *J. Am. Chem. Soc.* **2003**, *125*, 320−321.
(13) Yildiz, I.; McCaughan, B.; Cruickshank, S. F.; Callan, J. F.; Raymo, F. M. *Langmuir* **2009**, *25*, 7090−7096.

(14) Fafarman, A. T.; Koh, W. K.; Diroll, B. T.; Kim, D. K.; Ko, D. K.; Oh, S. J.; Ye, X. C.; Doan-Nguyen, V.; Crump, M. R.; Reifsnyder, D. C.; Murray, C. B.; Kagan, C. R. *J. Am. Chem. Soc.* **2011**, *133*, 15753−15761.
(15) Law, M.; Luther, J. M.; Song, O.; Hughes, B. K.; Perkins, C. L.; Nozik, A. J. *J. Am. Chem. Soc.* **2008**, *130*, 5974−5985.
(16) Foos, E. E. *J. Phys. Chem. Lett.* **2013**, *4*, 625−632.
(17) Frederick, M. T.; Amin, V. A.; Cass, L. C.; Weiss, E. A. *Nano Lett.* **2011**, *11*, 5455−5460.
(18) Liang, Y.; Thorne, J. E.; Parkinson, B. A. *Langmuir* **2012**, *28*, 11072−11077.
(19) Tan, Y.; Jin, S.; Hamers, R. J. *J. Phys. Chem. C* **2013**, *117*, 313−320.
(20) Schapotschnikow, P.; Hommersom, B.; Vlugt, T. J. H. *J. Phys. Chem. C* **2009**, *113*, 12690−12698.
(21) Aldana, J.; Wang, Y. A.; Peng, X. G. *J. Am. Chem. Soc.* **2001**, *123*, 8844−8850.
(22) Parak, W. J.; Gerion, D.; Pellegrino, T.; Zanchet, D.; Micheel, C.; Williams, S. C.; Boudreau, R.; Le Gros, M. A.; Larabell, C. A.; Alivisatos, A. P. *Nanotechnology* **2003**, *14*, R15−R27.
(23) Ewing, S. P.; Lockshon, D.; Jencks, W. P. *J. Am. Chem. Soc.* **1980**, *102*, 3072−3084.
(24) Dubois, F.; Mahler, B.; Dubertret, B.; Doris, E.; Mioskowski, C. *J. Am. Chem. Soc.* **2007**, *129*, 482−483.
(25) Querner, C.; Reiss, P.; Bleuse, J.; Pron, A. *J. Am. Chem. Soc.* **2004**, *126*, 11574−11582.
(26) Algar, W. R.; Krull, U. J. *ChemPhysChem* **2007**, *8*, 561−568.
(27) Frederick, M. T.; Amin, V. A.; Swenson, N. K.; Ho, A. Y.; Weiss, E. A. *Nano Lett.* **2013**, *13*, 287−292.
(28) Wang, J.; Xu, J.; Goodman, M. D.; Chen, Y.; Cai, M.; Shinar, J.; Lin, Z. *J. Mater. Chem.* **2008**, *18*, 3270−3274.
(29) Zhu, H.; Coleman, D. M.; Dehen, C. J.; Geisler, I. M.; Zemlyanov, D.; Chmielewski, J.; Simpson, G. J.; Wei, A. *Langmuir* **2008**, *24*, 8660−8666.
(30) Zhao, Y.; Perez-Segarra, W.; Shi, Q. C.; Wei, A. *J. Am. Chem. Soc.* **2005**, *127*, 7328−7329.
(31) Ito, S.; Murakami, T. N.; Comte, P.; Liska, P.; Gratzel, C.; Nazeeruddin, M. K.; Gratzel, M. *Thin Solid Films* **2008**, *516*, 4613−4619.
(32) Peng, Z. A.; Peng, X. G. *J. Am. Chem. Soc.* **2001**, *123*, 183−184.
(33) Yu, W. W.; Qu, L. H.; Guo, W. Z.; Peng, X. G. *Chem. Mater.* **2003**, *15*, 2854−2860.
(34) Guijarro, N.; Lana-Villarreal, T.; Mora-Sero, I.; Bisquert, J.; Gomez, R. *J. Phys. Chem. C* **2009**, *113*, 4208−4214.
(35) Pernik, D. R.; Tvrdy, K.; Radich, J. G.; Kamat, P. V. *J. Phys. Chem. C* **2011**, *115*, 13511−13519.
(36) Selinsky, R. S.; Ding, Q.; Faber, M. S.; Wright, J. C.; Jin, S. *Chem. Soc. Rev.* **2013**, *42*, 2963−2985.
(37) Frisch, M. J.; Trucks, G. W.; Schlegel, H. B.; Scuseria, G. E.; Robb, M. A.; Cheeseman, J. R.; Scalmani, G.; Barone, V.; Mennucci, B.; Petersson, G. A.; Nakatsuji, H.; Caricato, M.; Li, X.; Hratchian, H. P.; Izmaylov, A. F.; Bloino, J.; Zheng, G.; Sonnenberg, J. L.; Hada, M.; Ehara, M.; Toyota, K.; Fukuda, R.; Hasegawa, J.; Ishida, M.; Nakajima, T.; Honda, Y.; Kitao, O.; Nakai, H.; Vreven, T.; Montgomery, J. A., Jr.; Peralta, J. E.; Ogliaro, F.; Bearpark, M.; Heyd, J. J.; Brothers, E.; Kudin, K. N.; Staroverov, V. N.; Keith, T.; Kobayashi, R.; Normand, J.; Raghavachari, K.; Rendell, A.; Burant, J. C.; Iyengar, S. S.; Tomasi, J.; Cossi, M.; Rega, N.; Millam, J. M.; Klene, M.; Knox, J. E.; Cross, J. B.; Bakken, V.; Adamo, C.; Jaramillo, J.; Gomperts, R.; Stratmann, R. E.; Yazyev, O.; Austin, A. J.; Cammi, R.; Pomelli, C.; Ochterski, J. W.; Martin, R. L.; Morokuma, K.; Zakrzewski, V. G.; Voth, G. A.; Salvador, P.; Dannenberg, J. J.; Dapprich, S.; Daniels, A. D.; Farkas, O.; Foresman, J. B.; Ortiz, J. V.; Cioslowski, J.; Fox, D. J. *Gaussian 09*, Revision C.01; Gaussian, Inc., Wallingford, CT, 2010.
(38) Glendening, E. D.; Badenhoop, J. K.; Reed, A. E.; Carpenter, J. E.; Bohmann, J. A.; Morales, C. M.; Weinhold, F. *NBO 5.9*; Theoretical Chemistry Institute, University of Wisconsin: Madison, WI, 2012; http://www.chem.wisc.edu/~nbo5.
(39) Hogarth, G. *Prog. Inorg. Chem.* **2005**, *53*, 71−563.
(40) Shishkov, I. F.; Geise, H. J.; Van Alsenoy, C.; Khristenko, L. V.; Vilkov, L. V.; Senyavian, V. M.; Van der Veken, B.; Herrebout, W.; Lokshin, B. V.; Garkusha, O. G. *J. Mol. Struct.* **2001**, *567*, 339−360.
(41) Young, A. G.; Al-Salim, N.; Green, D. P.; McQuillan, A. J. *Langmuir* **2008**, *24*, 3841−3849.
(42) Coucouvanis, D. *Prog. Inorg. Chem.* **1970**, *11*, 233−371.
(43) Casas, J. S.; Sanchez, A.; Bravo, J.; Garciafontan, S.; Castellano, E. E.; Jones, M. M. *Inorg. Chim. Acta* **1989**, *158*, 119−126.
(44) Onwudiwe, D. C.; Ajibade, P. A. *Polyhedron* **2010**, *29*, 1431−1436.
(45) Sharma, C. P.; Kumar, N.; Khandpal, M. C.; Chandra, S.; Bhide, V. G. *J. Inorg. Nucl. Chem.* **1981**, *43*, 923−930.
(46) Zotti, G.; Vercelli, B.; Berlin, A.; Virgili, T. *J. Phys. Chem. C* **2012**, *116*, 25689−25693.
(47) Wills, A. W.; Kang, M. S.; Khare, A.; Gladfelter, W. L.; Norris, D. J. *ACS Nano* **2010**, *4*, 4523−4530.
(48) Beyramabadi, S. A.; Morsali, A.; Vahidi, S. H. *J. Struct. Chem.* **2012**, *53*, 665−675.
(49) Bawendi, M. G.; Kortan, A. R.; Steigerwald, M. L.; Brus, L. E. *J. Chem. Phys.* **1989**, *91*, 7282−7290.
(50) Norris, D. J.; Bawendi, M. G. *Phys. Rev. B* **1996**, *53*, 16338−16346.
(51) Xi, L.; Lek, J. Y.; Liang, Y. N.; Boothroyd, C.; Zhou, W.; Yan, Q.; Hu, X.; Chiang, F. B. Y.; Lam, Y. M. *Nanotechnology* **2011**, 22.
(52) Koole, R.; Schapotschnikow, P.; Donega, C. d. M.; Vlugt, T. J. H.; Meijerink, A. *ACS Nano* **2008**, *2*, 1703−1714.
(53) Liu, I. S.; Lo, H.-H.; Chien, C.-T.; Lin, Y.-Y.; Chen, C.-W.; Chen, Y.-F.; Su, W.-F.; Liou, S.-C. *J. Mater. Chem.* **2008**, *18*, 675−682.
(54) Munro, A. M.; Jen-La Plante, I.; Ng, M. S.; Ginger, D. S. *J. Phys. Chem. C* **2007**, *111*, 6220−6227.
(55) Wuister, S. F.; Donega, C. D.; Meijerink, A. *J. Phys. Chem. B* **2004**, *108*, 17393−17397.
(56) Ning, Z.; Molnar, M.; Chen, Y.; Friberg, P.; Gan, L.; Agren, H.; Fu, Y. *Phys. Chem. Chem. Phys.* **2011**, *13*, 5848−5854.
(57) Hammett, L. *J. Am. Chem. Soc.* **1937**, *59*, 96−103.
(58) Hansch, C.; Leo, A.; Taft, R. W. *Chem. Rev.* **1991**, *91*, 165−195.
(59) Puzder, A.; Williamson, A. J.; Zaitseva, N.; Galli, G.; Manna, L.; Alivisatos, A. P. *Nano Lett.* **2004**, *4*, 2361−2365.
(60) Galian, R. E.; Scaiano, J. C. *Photochem. Photobiol. Sci.* **2009**, *8*, 70−74.
(61) Landes, C.; Burda, C.; Braun, M.; El-Sayed, M. A. *J. Phys. Chem. B* **2001**, *105*, 2981−2986.
(62) Bullen, C.; Mulvaney, P. *Langmuir* **2006**, *22*, 3007−3013.
(63) Schlenoff, J. B.; Li, M.; Ly, H. *J. Am. Chem. Soc.* **1995**, *117*, 12528−12536.
(64) Chinwangso, P.; Jamison, A. C.; Lee, T. R. *Acc. Chem. Res.* **2011**, *44*, 511−519.
(65) von Wrochem, F.; Gao, D.; Scholz, F.; Nothofer, H.-G.; Nelles, G.; Wessels, J. M. *Nat. Nanotechnol.* **2010**, *5*, 618−624.
(66) Wessels, J. M.; Nothofer, H. G.; Ford, W. E.; von Wrochem, F.; Scholz, F.; Vossmeyer, T.; Schroedter, A.; Weller, H.; Yasuda, A. *J. Am. Chem. Soc.* **2004**, *126*, 3349−3356.